Normal modes of a Tesla magnifier

Bart H. McGuyer

https://bartmcguyer.com/notes/note-16-MagnifierModes.pdf

(Dated: July 2, 2024. Revision: September 7, 2024.)

TL;DR: Exploration of the normal modes and limiting behavior of a transmission line with two capacitive loads: one internal and the other terminating. Provides a toy model for an interesting variant of a Tesla coil called a Tesla magnifier.

There's a three-circuit variation of a Tesla transformer (or Tesla coil) nicknamed a Tesla magnifier.[1,2] As sketched in Fig. 1, it differs from a traditional two-circuit Tesla coil by the addition of a "tertiary" circuit directly connected to the output of the secondary circuit. Researchers have explored similar triple-resonance Tesla transformers as pulsed-power supplies to produce very high voltages.[3–6] Tesla-coil enthusiasts have built many to produce long sparks, but seem to regard them as difficult to design and tune. One practical advantage is that they allow a good separation between the final output portion and the rest of a system.

This note presents a simple model to calculate the standing-wave resonances (or normal modes) of the coupled secondary and tertiary system. It does this by approximating both circuits as transmission lines[2,7,8] and their connection as a lumped capacitance, as sketched in Fig. 1. It uses this model to explore how the connection's capacitance alters the modes of a quarter-wave resonator in general, and to analyze a specific, well-documented magnifier. The current profiles of the resonances provide an example of a nonharmonic Fourier series.[9] The modes and how they vary as the loads change are indeed complicated, but their limiting behavior, especially when one or both loads are large, seems to provide a reasonably intuitive way to qualitatively understand them.

CONTENTS

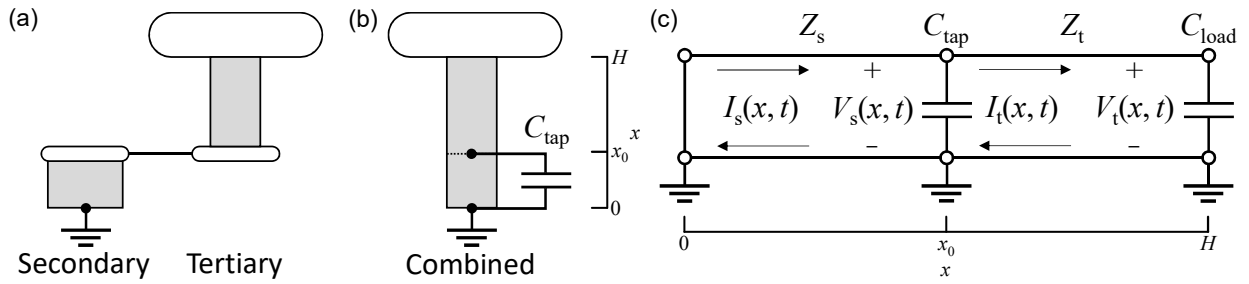

FIG. 1. Modeling approach. (a) Side profile of original secondary and tertiary circuits, showing single-layer solenoids and electrodes. (b) Approximating the secondary-tertiary interface with a lumped capacitor. (c) Transmission-line model for the combined secondary and tertiary system.

I. MODEL

A. General case of nonidentical lines

Consider two segments of ideal, lossless transmission lines, as sketched in Fig. 1. Let's label the first segment corresponding to the secondary with "s" and the second corresponding to the tertiary with "t." Within each line, the voltage $V_j(x,t)$ and current $V_j(x,t)$ are coupled by Telegraphers' equations,

$$\frac{\partial V_j(x,t)}{\partial x} = -l_j \frac{\partial I_j(x,t)}{\partial t} \tag{1}$$

$$\frac{\partial I_j(x,t)}{\partial x} = -c_j \frac{\partial V_j(x,t)}{\partial t}, \tag{2}$$

for $j = s$ or t, where l_j and c_j are distributed series inductances and shunt capacitances for each line segment. By convention, positive current $I_j(x,t)$ flows towards increasing x.

The boundary condition at the bottom ($x = 0$) is a short circuit, $V_s(0,t) = 0$. The boundary condition at the top ($x = H$) is a capacitive load, C_{load}, or "topload" for short. Since we are interested in lossless normal modes (standing-wave resonances), we may consider harmonic voltages and currents proportional to $e^{i\omega t}$ with angular frequency $\omega > 0$. Then the top boundary condition is

$$I_t(H,t) = C_{\text{load}} \frac{d}{dt} V_t(H,t). \tag{3}$$

For the limiting case of vanishing $C_{\text{load}} \longrightarrow 0$, this condition becomes $I_t(H,t) = 0$. Likewise, for infinite $C_{\text{load}} \longrightarrow \infty$, it becomes $V_t(H,t) = 0$.

At the interface between the secondary and tertiary circuits, the electrodes and direct connection contribute an effective lumped capacitance C_{tap}. To approximate this, the interface between the secondary and tertiary segments at the tap ($x = x_0$) has the conditions

$$V_s(x_0,t) = V_t(x_0,t) \tag{4}$$

$$I_s(x_0,t) - I_t(x_0,t) = C_{\text{tap}} \frac{d}{dt} V_s(x_0,t). \tag{5}$$

For the limiting case of vanishing $C_{\text{load}} \longrightarrow 0$, which removes the tap, the current condition becomes $I_s(x_0, t) = I_t(x_0, t)$. Likewise, for infinite $C_{\text{load}} \longrightarrow \infty$, which severs the interface, both conditions reduce to only one, $V_s(H, t) = V_t(H, t) = 0$.

For the secondary segment, the bottom boundary condition is satisfied by the forms

$$V_s(x, t) = V_s \sin(k_s x) e^{i\omega t} \tag{6}$$

$$I_s(x, t) = I_s \cos(k_s x) e^{i\omega t}, \tag{7}$$

where V_s and I_s are complex amplitudes (phasors) and ω is a positive angular frequency. From the Telegraphers' equations, the wavenumber $k_s = \pm\omega\sqrt{l_s c_s}$, where the choice of sign affects the signs of the phasors and the impedances they model. To be cautious, let's leave the choice of sign free and return to it later. Then, from the Telegrapher's equations, the corresponding characteristic impedance $Z_s = V_s/I_s = -i\omega l_s/k_s = k_s/(i\omega c_s) = \mp i\sqrt{l_s/c_s}$.

For the tertiary segment, we need an additional parameter beyond the wavenumber to have two degrees of freedom. The following forms are convenient

$$V_t(x, t) = V_t \cos[k_t(H' - x)] e^{i\omega t} \tag{8}$$

$$I_t(x, t) = I_t \sin[k_t(H' - x)] e^{i\omega t}, \tag{9}$$

where again V_t and I_t are phasors. Here, the additional parameter H' will be set by the top boundary condition, and equals H in the limit of $C_{\text{load}} \longrightarrow \infty$. Note that H' is not unique up to adding integer multiples of π/k_t, which just shifts the profile and occasionally changes the signs of the phasors. Similar to the first segment, the wavenumber $k_t = \pm\omega\sqrt{l_t c_t}$ and the corresponding characteristic impedance $Z_t = V_t/I_t = -i\omega l_t/k_t = k_t/(i\omega c_t) = \mp i\sqrt{l_t/c_t}$.

With these forms, the top boundary condition becomes

$$\tan[k_t(H' - H)] = i\omega C_{\text{load}} Z_t. \tag{10}$$

However, the right hand side is not constant with ω or k_t. Substituting for Z_t gives

$$\frac{\tan[k_t(H' - H)]}{k_t} = \frac{C_{\text{load}}}{c_t}, \tag{11}$$

where now the right hand side is a fixed ratio. Tangent is an odd function, so for a fixed sign of $H' - H$, the sign of k_t does not matter.

Similarly, the interface conditions become

$$V_s \sin(k_s x_0) = V_t \cos[k_t(H' - x_0)] \tag{12}$$

$$I_s \cos(k_s x_0) - I_t \sin[k_t(H' - x_0)] = i\omega C_{\text{tap}} V_s \sin(k_s x_0). \tag{13}$$

Dividing the second by $V_s \sin(k_s x_0)$ and using the first gives

$$\frac{1}{Z_s} \cot(k_s x_0) - \frac{1}{Z_t} \tan[k_t(H' - x_0)] = i\omega C_{\text{tap}}. \tag{14}$$

Using $i\omega Z_s = k_s/c_s$ and $Z_s/Z_t = c_t k_s/(c_s k_t)$, this interface condition simplifies to

$$\frac{\cot(k_s x_0)}{k_s} - \left(\frac{c_t}{c_s}\right) \frac{\tan[k_t(H' - x_0)]}{k_t} = \frac{C_{\text{tap}}}{c_s}. \tag{15}$$

Noting that both tangent and cotangent are odd functions, we see that the signs of k_s and k_t do not affect this equation, so long as the sign of $H' - x_0$ is fixed.

Pulling everything together, a first form for the model is given by the system

$$\frac{\tan\left[\left(\frac{H'_n}{H} - 1\right) k_{t,n} H\right]}{k_{t,n} H} = \frac{C_{\text{load}}}{c_t H}, \tag{16}$$

$$\frac{\cot(k_{s,n} x_0)}{k_{s,n} x_0} - \left(\frac{c_t H}{c_s x_0}\right) \frac{\tan\left[\left(\frac{H'_n}{H} - \frac{x_0}{H}\right) k_{t,n} H\right]}{k_{t,n} H} = \frac{C_{\text{tap}}}{c_s x_0}, \tag{17}$$

$$\frac{k_{s,n}}{k_{t,n}} = \frac{c_s Z_s}{c_t Z_t} = \text{sgn}(k_{s,n} k_{t,n}) \sqrt{\frac{l_s c_s}{l_t c_t}}, \tag{18}$$

where x_0, H, c_s, c_t, Z_s, Z_t, (or l_s, l_t,) C_{tap}, and C_{load} are known inputs. In general, there will be multiple solutions, so the wavenumbers $k_{j,n}$ and parameters H'_n now have an explicit mode index $n = 1, 2, 3, \ldots$ in their subscripts. The first line of the system is the top boundary condition, which gives H'_n from the other parameters. Note that tangent is periodic to translations by π, so there are multiple solutions for H'_n. However, each solution has an equivalent effect on the next line. The second line is the interface condition, which is a transcendental equation. It lets you solve for both wavenumbers for all modes, given their relationship by definition in the third line, the last part of which depends on the relative sign of the two wavenumbers. Here, and subsequently, let's choose positive wavenumbers, since this sign does not matter.

Finally, it's a little more convenient for numerical use if we introduce the following capacitances and inductances for the segments,

$$C_s = c_s x_0, \qquad L_s = l_s x_0, \qquad C_t = c_t (H - x_0), \qquad \text{and} \qquad L_t = l_t (H - x_0), \tag{19}$$

then, after rearranging and choosing positive wavenumbers, the system becomes

$$\frac{\tan\left[\left(\frac{H'_n}{H} - 1\right) k_{t,n} H\right]}{k_{t,n} H} = \frac{C_{\text{load}}}{C_t} \left(1 - \frac{x_0}{H}\right), \tag{20}$$

$$\cot\left[\frac{k_{t,n} H}{\alpha} \left(1 - \frac{x_0}{H}\right)\right] - \sqrt{\frac{L_s C_t}{L_t C_s}} \tan\left[\left(\frac{H'_n}{H} - \frac{x_0}{H}\right) k_{t,n} H\right] = \frac{k_{t,n} H}{\alpha} \left(1 - \frac{x_0}{H}\right) \left(\frac{C_{\text{tap}}}{C_s}\right), \tag{21}$$

$$\alpha\, k_{s,n} x_0 = k_{t,n} (H - x_0), \tag{22}$$

$$\text{where} \quad \alpha = \sqrt{\frac{L_t C_t}{L_s C_s}} = \sqrt{\frac{l_t c_t}{l_s c_s}} \left(\frac{H}{x_0} - 1\right). \tag{23}$$

The first line gives H'_n/H as a function of $k_{t,n} H$, C_{load}/C_t, and x_0/H. Without loss of generality, we may choose the solutions

$$\frac{H'_n}{H} = 1 + \frac{\arctan\left[k_{t,n} H \left(\frac{C_{\text{load}}}{C_t}\right) \left(1 - \frac{x_0}{H}\right)\right]}{k_{t,n} H} \geq 1, \tag{24}$$

with equality occurring if $C_{\text{load}} = 0$ or $n \longrightarrow \infty$. Using this, the second line gives $k_{n,t}H$ as a function of x_0/H, C_{tap}/C_s, C_{load}/C_t, the electrical-length-ratio parameter α, and the impedance ratio $\sqrt{L_s C_t/(L_t C_s)} = |Z_s/Z_t|$. The other wavenumbers follow from the third and fourth lines.

Last, but not least, the resonant frequencies for the modes are

$$\omega_n = \frac{k_{s,n}}{\sqrt{l_s c_s}} = \frac{k_{s,n}x_0}{\sqrt{L_s C_s}} = \frac{k_{t,n}}{\sqrt{l_t c_t}} = \frac{k_{t,n}(H - x_0)}{\sqrt{L_t C_t}}, \tag{25}$$

from the Telegraphers' equations.

B. Spatial profiles and orthogonality

After solving, the spatial variations (or profiles) of voltage and current follow from their forms (6–9) and the original interface conditions, which give the ratios

$$\frac{V_{t,n}}{V_{s,n}} = \frac{\sin(k_{s,n}x_0)}{\cos[k_{t,n}(H'_n - x_0)]} \tag{26}$$

$$\frac{I_{t,n}}{I_{s,n}} = \frac{\cos(k_{s,n}x_0) - \left(\frac{C_{\text{tap}}}{C_s}\right) k_{s,n}x_0 \sin(k_{s,n}x_0)}{\sin[k_{t,n}(H'_n - x_0)]}, \tag{27}$$

where the phasors now include an explicit mode index in their subscripts. The second term in the numerator of the current ratio creates a discontinuity to account for the current diverted to the tap capacitance.

Before we continue, it's worth pausing to capture how orthogonality works for the spatial profiles of voltage and current. First, some background: For typical standing-wave resonances on a uniform, lossless line with simple open- or short-circuit terminations, the voltage and current profiles correspond to terms in harmonic Fourier series (sinusoidal terms with harmonically related arguments). Together, all of the voltage profiles form an orthogonal basis for $V(x,t)$, and likewise, all of the current profiles for $I(x,t)$. This orthogonality it not just a mathematical convenience, but is also physically required by energy conservation: Each resonance evolves independently from all others, so its energy cannot depend on any other resonances. Therefore, the voltage profile and current profile for each resonance must contribute independently to the total instantaneous energy stored by the line,

$$U(t) = \frac{1}{2}\int_0^H \left[l(x)I(x,t)^2 + c(x)V(x,t)^2\right] dx, \tag{28}$$

which occurs if all of the voltage profiles are mutually orthogonal, and all of the current profiles are mutually orthogonal, in the above integral.

Here, however, we attached external capacitors to the lines, which store energy that's not included in (28) when the voltages across them are nonzero and they have nonzero capacitance. In this case, energy conservation still requires the the current profiles to be orthogonal, but curiously, it requires the voltage profiles to be typically nonorthogonal. This also applies to the profiles along the secondary of a Tesla coil (see Ref. 7), and is discussed

more generally towards the end of Ref. 9. In both cases, the current series is a nonharmonic Fourier series (sinusoidal terms without harmonically related arguments). The appropriate inner product for the current orthogonality follows from (28), which was written to allow spatially varying line parameters. For two profiles $I_a(x)$ and $I_b(x)$, this inner product is proportional to

$$\int_0^H l(x)I_a(x)I_b(x)dx = l_s\int_0^{x_0} I_a(x)I_b(x)dx + l_t\int_{x_0}^H I_a(x)I_b(x)dx. \tag{29}$$

Alternatively, you can show that the forms (6–9) are orthogonal after substitution as follows. For the first integral, pull out a common factor of $V_a(x_0)V_b(x_0)$. For the second integral, note that half of the terms cancel using (11) and pull out the same factor $V_a(x_0)V_b(x_0)$ from the remaining half. Combine terms and convert them to resemble the left side of (15). Then, noting that the right hand side of (15) is the same for "a" and "b", everything cancels.

C. Special case of identical lines

For identical lines, $l_s = l_t$, $c_s = c_t$, and $Z_s = Z_t$, so $k_{s,n} = k_{t,n}$. To simplify notation, let's introduce a single wavenumber,

$$k_n = k_{s,n} = k_{t,n}, \tag{30}$$

and an effective lumped capacitance for the entire line,

$$C_0 = c_s H = C_s + C_t. \tag{31}$$

The model then simplifies to the system

$$\frac{\tan\left[\left(\frac{H'_n}{H}-1\right)k_nH\right]}{k_nH} = \frac{C_{\text{load}}}{C_0}, \tag{32}$$

$$\cot\left[\left(\frac{x_0}{H}\right)k_nH\right] - \tan\left[\left(\frac{H'_n}{H}-\frac{x_0}{H}\right)k_nH\right] = k_nH\left(\frac{C_{\text{tap}}}{C_0}\right). \tag{33}$$

The first line gives H'_n/H as a function of k_nH and C_{load}/C_0, which is

$$\frac{H'_n}{H} = 1 + \frac{\arctan\left[k_nH\left(\frac{C_{\text{load}}}{C_0}\right)\right]}{k_nH} \geq 1, \tag{34}$$

with equality occurring if $C_{\text{load}} = 0$ or $n \longrightarrow \infty$. Using this, the second line gives k_nH as a function of x_0/H, C_{tap}/C_0, and C_{load}/C_0. If there is no topload ($C_{\text{load}} = 0$), then $H'_n = H$ and the second line reduces to

$$\cot\left[\left(\frac{x_0}{H}\right)k_nH\right] - \tan\left[\left(1-\frac{x_0}{H}\right)k_nH\right] = k_nH\left(\frac{C_{\text{tap}}}{C_0}\right), \tag{35}$$

which gives k_nH as a function of x_0/H and C_{tap}/C_0.

As a sanity check, note that if the tap is placed at the top ($x_0 = H$), then the system reduces to the boundary condition of a line with a capacitive load,

$$(k_n H)\tan(k_n H) = \frac{C_0}{C_{\text{load}} + C_{\text{tap}}}, \tag{36}$$

which is a simple model of a Tesla transformer (see Ref. 7). Likewise, if the tap is placed at the bottom ($x_0 = 0$), then the system again reduces to this simple model, but with the value of C_{tap} removed. To see this, note that $\tan(k_n H'_n)$ diverges by design.

D. Corresponding cases of identical and nonidentical lines

The case of identical lines seems to have relatively clear limiting behavior, as we'll see below. Conveniently, there is a way to approximate a nonuniform line with a nearly equivalent uniform line, which provides a opportunity to understand complicated nonuniform lines via simpler uniform lines. This approximation isn't valid in general, but seems to work well for most cases of interest (lowest few modes for small x_0/H with $L_s \lesssim L_t$ and little influence from C_s). Intuitively, it's inspired by connecting different lines that should have similar low-frequency, conventional equivalent circuits for the lowest two resonances.

In detail, the approximation comes from removing the ratio of distributed capacitances in (15). Assuming the electrical length of the secondary is small, or $|k_{s,n} x_0| \ll 1$, then we can use $\cot(x) \approx 1/x$ for $|x| \ll 1$ and multiply all terms by c_s/c_t, so that the cotangent term on the left becomes $c_s/(c_t k_{s,n}^2 x_0)$. If we redefined this as $1/(k_{t,n}^2 x_0^*)$ for a new effective value of x_0^*, then we could convert it back to a cotangent. Eq. (15) then has a single value of k, just like a uniform line. Completing the rest of the derivation above gives a model for a uniform line with the following parameters,

$$k^* \approx k_{t,n} \tag{37}$$

$$x_0^* = (l_s/l_t) x_0 \tag{38}$$

$$H^* = H + x_0^* - x_0 \tag{39}$$

$$H_n'^* \approx H'_n + x_0^* - x_0 \tag{40}$$

$$c^* = c_t \tag{41}$$

$$C_0^* = c_t H^* = C_t + C_s \left(\frac{l_s c_t}{l_t c_s} \right) \tag{42}$$

where the addition of stars on the left sides denote effective uniform-line parameters. Note that $H_n'^*$ still follows from (34) using these new parameters.

The two relationships above that are approximately equal indicate that the final values of those quantities come from solving the uniform-line system. That is, while they're equal during the derivation of the above, their final values will differ from the corresponding nonuniform-line values at the level of this approximation's inaccuracy. In contrast, the other lines with equal signs are input parameters to that system.

All together, when this approximation is valid, you can construct the dimensionless ratios x_0^*/H^*, C_{load}/C_0^*, and C_{tap}/C_0^* that describe the effective, equivalent uniform line for the

nonuniform line. Physically, this approximation is equivalent to making a nonuniform line uniform in two steps: (1st) by stretching the secondary so that the distributed inductance matches the tertiary, $l_s \to l_s^* = l_t$, while keeping L_s unchanged, and (2nd) by discontinuously setting the distributed capacitance to be the same, $c_s \to c_s^* = c_t$. In the conventional equivalent circuit, this corresponds to keeping $C_t, L_t, L_s, C_{\text{tap}}$, and C_{load} fixed, and assuming C_s (or any resulting change to it) is not important.

II. NUMERICAL RESULTS

A. Identical lines without a toploaded

Let's begin with the "unloaded" case of identical lines with no toploaded ($C_{\text{load}} = 0$), which is modeled by (35). Fig. 2 shows two types of plots of numerical solutions for the first few wavenumbers k_n of the whole line. In all plots, the wavenumbers are shown as $(2/\pi)k_nH$, so that unloaded quarter-wave solutions correspond to odd numbers: $(2/\pi)k_nH = 2n-1 = 1, 2, 3, \ldots$ The colorful curves are the solutions, and the dashed horizontal lines with matching colors that the curves start from on the left are their corresponding quarter-wave modes.

The first type of plot shows the variation with the position of the tap (shown as x_0/H), for a few fixed sizes of the tap capacitance (C_{tap}/C_0). For zero tap capacitance, the solutions are the quarter-wave modes. For small tap capacitance, the top left plot shows that the wavenumbers begin to deviate if the tap position is not positioned at a quarter-wave voltage node. As the tap capacitance increases, the middle and bottom left plots show that these deviations asymptote to the following three cases indicated by several dashed curves.

The first limiting case, indicated by a grey dot-dashed curve, corresponds to a lumped LC resonance of the tap capacitance with an effective inductance for the line. We can model this resonance using $k = \omega\sqrt{lc}$ for the line, $\omega = 1/\sqrt{LC}$ for a lumped LC circuit, and then $C \approx C_{\text{tap}} + C_s$ and $L \approx L_s$, which gives

$$k_{\text{tap}}^{\{L_s\}} \approx \frac{1}{H}\sqrt{\left(\frac{H}{x_0}\right)\left(\frac{C_0}{C_{\text{tap}}}\right)}, \tag{43}$$

where the approximation assumes $C_{\text{tap}} \gg C_s$.

The other two limiting cases, indicated by the black dashed curves, correspond to the limit of an infinite tap capacitance, which severs the line at the tap. This turns the secondary into an isolated half-wave resonator of length x_0, which has the modes

$$k_{s,n}^{\{\text{cut},\,\lambda/2\}} = \pi n/x_0, \tag{44}$$

and turns the tertiary into an isolated quarter-wave resonator of length $H - x_0$, for which

$$k_{t,n}^{\{\text{cut},\,\lambda/4\}} = (2n-1)\pi/[2(H-x_0)]. \tag{45}$$

To help differentiate between the two, the curves for $k_{s,n}^{(\text{cut})}$ are dot-dashed and those for $k_{t,n}^{(\text{cut})}$ are dashed. In the plots on the left side, the curves are also distinguishable because

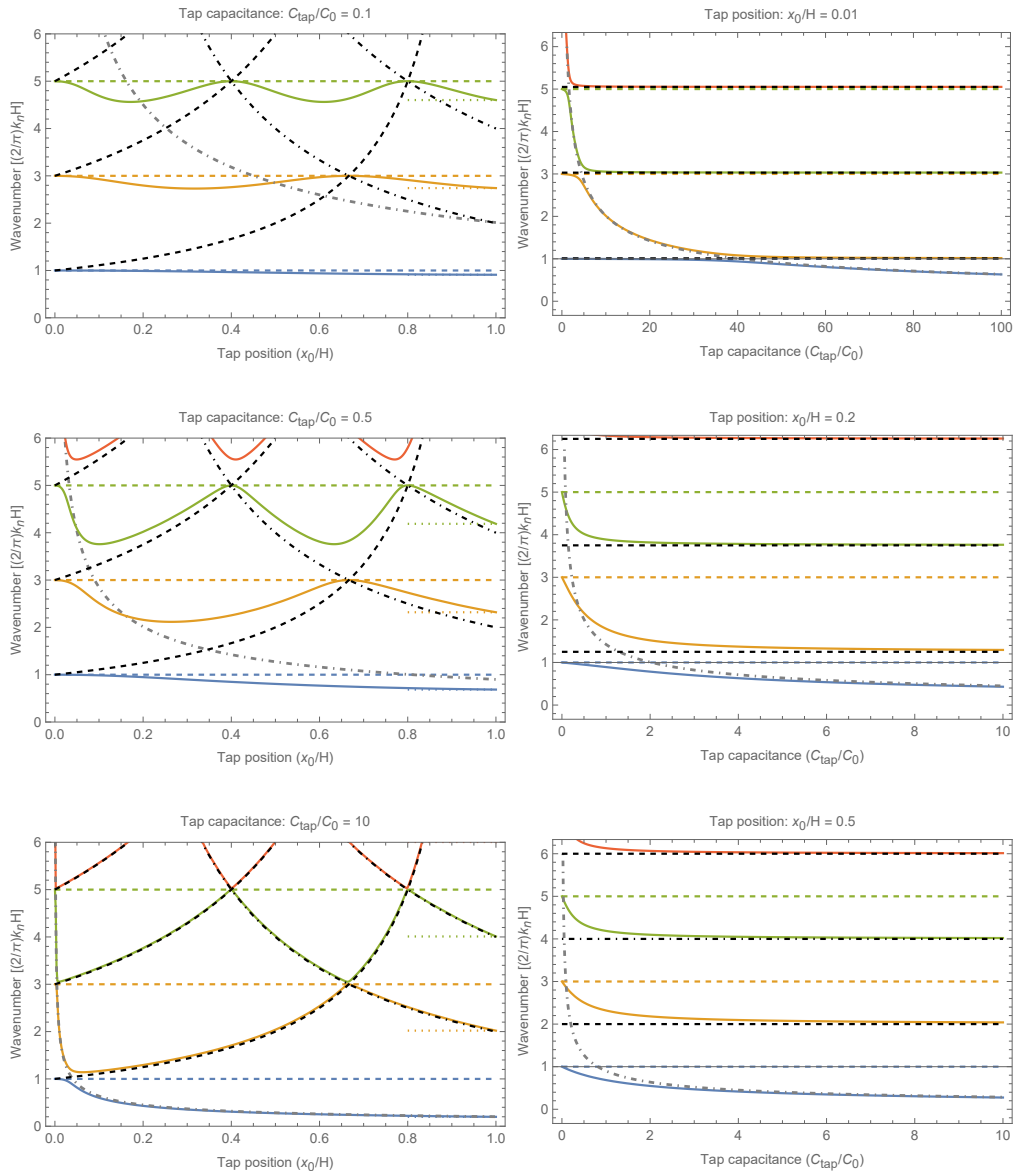

FIG. 2. Identical lines without a toploads. Solid curves are solutions of (35) for the first few wavenumbers k_n for the entire line. The left (right) column shows the solutions for fixed tap capacitance (position) as a function of tap position (capacitance). For reference, colorful horizontal lines indicate quarter-wave modes: full-width dashed for unloaded, and only on the left, partial-width dotted for loaded modes of (36) with $C_{\text{load}} = 0$. The grey dot-dashed curves are the lumped mode of (43). The black dot-dashed curves are the cut-segment modes of (44), and the dashed of (45).

those for $k_{s,n}^{(\text{cut})}$ diverge as $x_0 \to 0$, and those for $k_{t,n}^{(\text{cut})}$ as $x_0 \to H$. Note that these limiting curves intersect the unloaded quarter-wave modes at their voltage nodes, creating interesting regions of near degeneracy about those intersections.

Additionally, as the tap position nears the top, the wavenumbers asymptote to the loaded quarter-wave modes of (36) with $C_{\text{load}} = 0$, as expected, which are indicated by partial-width

horizontal dotted lines with colors matching the wavenumber curves. As the tap capacitance increases, the loaded quater-wave modes themselves asymptote to coincide with the half-wave modes (44) at $x_0 = H$.

The second type of plot shows the variation with the size of the tap capacitance, for a few fixed tap positions. These are shown on the right in Fig. 2, and have all the same curves as those on the left. Since the tap position is fixed, the infinite-tap-capacitance limiting cases are now horizontal lines. The lumped resonance (43) is still a curve, and the top right plot shows the hybridization it causes as it passes through the wavenumbers, which is harder to see in the other plots.

Exploring the voltage and current spatial profiles, the results are similar to expectations, with the shapes stretching between unloaded quarter- and half-wave solutions as they near odd and even numbers, respectively, but their joining across the tap has surprises, especially for current. When there are narrow avoided crossings where the dashed limiting curves intersect, such as shown in the top right of Fig. 2, there are interesting cases of pairs of neighboring modes having a hybridized appearance.

Of particular interest is the regime of large tap capacitance. Generally, this tends to produce a prolonged hybridization of the two lowest modes, giving profiles like those shown in Fig. 3. This is because the lumped mode (43) eventually stretches the fundamental

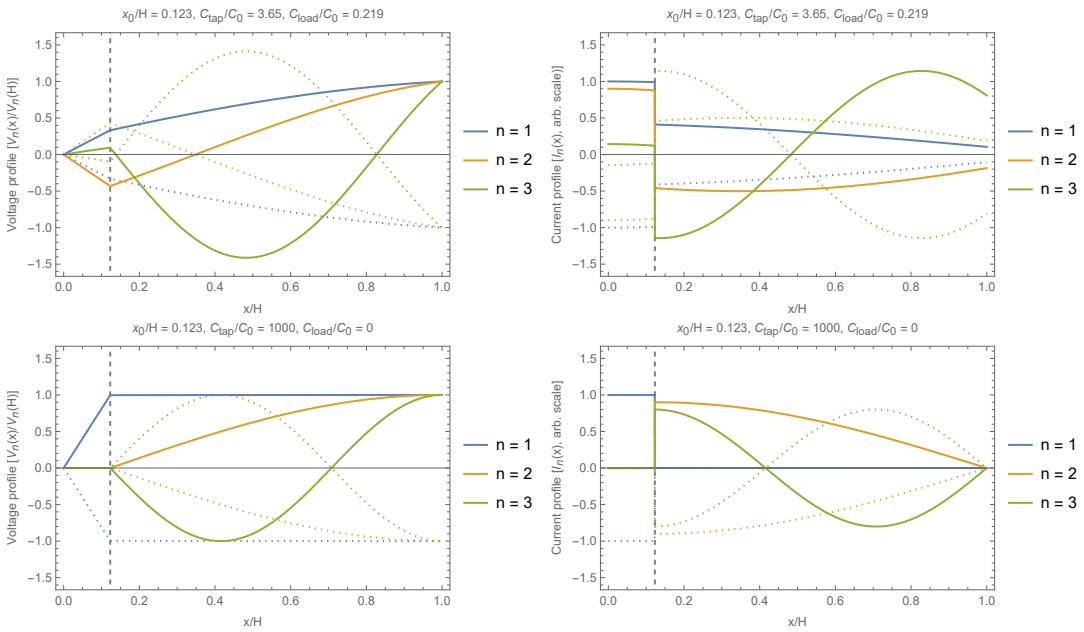

FIG. 3. Voltage (left) and current (right) spatial profiles of identical lines with large tap capacitance. (Top row) Identical line with parameters that correspond to the nonidentical "3:4:5" magnifier example given later. The profiles strongly resemble those in Fig. 5. The hybridized appearance of the two lowest modes often occurs in the large-tap regime (e.g., similar profiles result near the avoided crossing in the top right of Fig. 2 with $x_0/H = 0.01$ and $C_{\text{tap}}/C_0 = 40$). (Bottom row) Effect of modifying the line to have a significantly larger tap and no toploads. Notice that the profiles are still qualitatively similar, despite the large tap effectively severing the line.

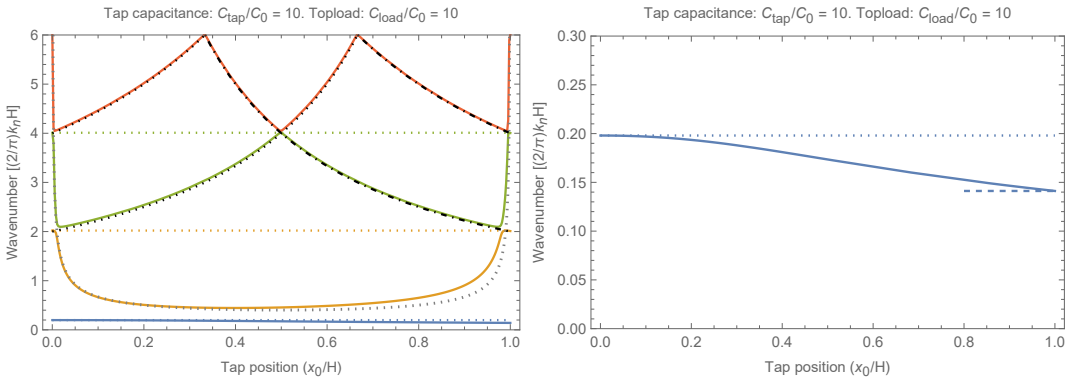

FIG. 4. Identical lines with a topload. (Left) Solid curves are solutions of (32) and (33) for the first few wavenumbers k_n for the entire line. For reference, dotted horizontal lines indicate loaded quarter-wave modes of (36) with $C_{\text{tap}} = 0$. The grey dotted curve is the lumped mode of (47). The black dot-dashed curves are the cut segment modes of (45), and the dotted of (46). (Right) Highlight of k_1, which transitions between loaded quarter-wave modes (36) with $C_{\text{tap}} = 0$ on the left and with $C_{\text{tap}} \neq 0$ on the right, shown with a partial-width dashed line.

quarter-wave mode towards the lumped limit of spatially constant current and roughly linearly varying voltage, just like for a large topload in a Tesla coil. However, for a Tesla magnifier, this regime has not one but effectively two such lumped modes, because the two lowest modes both have wavenumbers near or below the quarter-wave limit. As a result, to maintain orthogonality, the current profiles usually are sum and difference combinations (hybridizations) of the currents in the secondary and tertiary, as shown. The corresponding voltage profiles tend to resemble 1/4- and 3/4-wave modes, despite both being effectively 1/4-wave or lower modes. Eventually, however, an infinite tap capacitance effectively severs the line, making the two lowest modes correspond to current only in the secondary or tertiary.

B. Identical lines with a topload

Continuing from above, let's consider the "loaded" case of a nonzero topload ($C_{\text{load}} \neq 0$), which is modeled by (32) and (33). Fig. 4 shows two related plots of numerical solutions for the first few wavenumbers k_n of the whole line. The colorful curves are the solutions, and the dotted horizontal lines with matching colors are their corresponding loaded quarter-wave modes of (36) for $C_{\text{tap}} = 0$, which for large C_{load} asymptote to half-wave modes.

Both plots highlight what seems to be the limiting behavior when both the tap and topload capacitances are much larger than C_0. The right plot highlights the lowest mode, and shows its transition from a loaded quarter-wave mode of (36) with $C_{\text{tap}} = 0$ on the left, to one with $C_{\text{tap}} \neq 0$ on the right. The left plot shows limiting cases for the higher modes. The cut secondary modes of (44) are unchanged. However, increasing the topload smoothly transitions the cut tertiary modes from the previous quarter-wave model of (45)

to a half-wave model given by

$$k_{t,n}^{\{\mathrm{cut},\,\lambda/2\}} = \pi n/(H - x_0), \tag{46}$$

shown with the black dotted curves. The previous lumped resonance of (43) seems to become similar to an LC resonance of the C_{tap} with both L_s and L_t in parallel,

$$k_{\mathrm{tap}}^{\{L_s \| L_t\}} \approx \frac{1}{H}\sqrt{\left(\frac{1}{x_0/H} + \frac{1}{1 - x_0/H}\right)\left(\frac{C_0}{C_{\mathrm{tap}}}\right)}, \tag{47}$$

shown with the grey dotted curve, though not perfectly since this ignores C_{load}. (Note the missed intersection with the lowest avoided crossing on the right.) For an improved lumped model that agrees well with both of the lowest two curves, please see Ref. 2.

C. Nonidentical lines example of a real magnifier

Finally, let's explore the magnifier described in Ref. 11. That reference provides the most detailed documentation I've found of a magnifier. For additional comparison, Ref. 10 provides theoretical results from a simulation of this magnifier using a much more realistic transmission-line-style model than the uniform-line toy-model approach considered here.

The "3:4:5" magnifier in Ref. 11 was designed to transfer all of the energy from a capacitor in its primary circuit to the effective output capacitance of the tertiary using a design process outlined in Ref. 12, which builds on Ref. 3. For this particular magnifier, this involved adjusting the lowest three normal modes of the entire magnifier (primary, secondary, and tertiary circuits) to have resonant frequencies with relative ratios of 3 to 4 to 5.

To proceed, we need to compile parameters for the 3:4:5 magnifier from Ref. 11: The secondary height is $x_0 = 10.2$ cm. The tertiary height wasn't stated, but estimating it both from a description of its winding[13] with its inductance, and from its diameter[13] and apparent aspect ratio in a picture, gives $H - x_0 \approx 32.4 \pm 0.4$ cm. Thus $H \approx 42.6$ cm and the tap position ratio $x_0/H \approx 0.24$. The low-frequency inductances are $L_s = 3.948$ mH and $L_t = 28.2$ mH. The calculated Medhurst capacitances are 7.1 pF for the secondary and 5.6 pF for the tertiary. Following Ref. 14, we can roughly estimate the uniform capacitances as three times the Medhurst capacitances, giving $C_s \approx 21.3$ pF and $C_t \approx 16.8$ pF. All together, the parameter $\alpha \approx 2.37$. The remaining two capacitances are harder to estimate. For the topload, the stated effective capacitance of $C_{\mathrm{load}} + C_t^{\{\mathrm{Medhurst}\}} \approx 9.8$ pF, so $C_{\mathrm{load}} \approx 4.2$ pF. However, the simulation of Ref. 10 said adding 2 pF improved agreement, so let's use $C_{\mathrm{load}} = 6.2$ pF. For the tap, the stated effective capacitance of $C_{\mathrm{tap}} + C_s^{\{\mathrm{Medhurst}\}}$ + (unknown tertiary and other contributions) ≈ 79.64 pF for a 62 pF lumped tap capacitor. For our use, we need to remove direct contributions from the secondary and tertiary,[2] but keep any other contributions. However, let's again follow the simulation of Ref. 10, which found good agreement with $C_{\mathrm{tap}} = 70$ pF.

Table I shows that these parameter reproduce the first few resonant frequencies $f = \omega/(2\pi)$ measured and previously simulated reasonably well. This is actually surprising, because this work neglects the primary circuit, while the other values do not. Fortunately,

TABLE I. Comparison of the lowest resonant frequencies of the 3:4:5 magnifier. The results of this work agree reasonably well, except for missing a resonance from neglecting the primary circuit.

Source	f_a (kHz)	f_b (kHz)	f_c (kHz)	f_d (kHz)	System
Experiment (Ref. 11):	232	307	385	–	Primary, secondary, and tertiary.
Simulation (Ref. 10):	227	303	383	873	Primary, secondary, and tertiary.
This work:	227	–	361	922	Secondary and tertiary only.

including the primary circuit, which had $L_p = 62.02$ μH, $C_p = 5.08$ nF, and a self resonance at about 284 kHz, seems to have mainly produced the resonance near 307 kHz, with little perturbation to the other lowest modes. The remaining frequencies correspond closely to the first three normal modes of the isolated secondary-tertiary system. (For a comparison with a lumped-element model, please see Ref. 2.)

Figure 5 shows the profiles for the first three secondary-tertiary normal modes, as well as an approximation of the primary driven mode's voltage profile. The shapes of the normal modes agree reasonably well with those predicted in Ref. 10. Though their voltage profiles loosely resemble 1/4-, 3/4-, and 5/4-wave mode shapes, the ratios $k_{t,n}/k_{t,1} \approx \{1, 1.59, 4.06, 6.96, 7.82, 10.01, 13.11, 15.29, 16.25, \ldots\}$ shows clear deviations from the ideal quarter-wave ratios of $\{1, 3, 5, 7, 9, 11, 13, 15, 17, \ldots\}$. In particular, the second mode (corresponding to f_c) is very nearly another 1/4-wave mode, despite the resemblance of its voltage profile to a 3/4-mode shape (as anticipated from earlier).

The crude approximation of the primary-driven mode comes from appealing to lumped LC circuits: Assuming the primary induces the same electromotive force, each mode contributes a voltage proportional to $1/[1-(\omega/\omega_n)^2]$. Keeping only the first two modes, and accounting for the sign flip in the current profile for the second mode, leads to the superposition shown in the bottom of Fig. 5. The fact that the voltage profile for this mode resembles another 3/4-wave mode follows from this superposition, which seems to explain the curious appearance of a mode doubling in Ref. 10's results. However, the current profile (not shown) that follows from this approximation does not agree well. This disagreement likely follows from not reproducing the voltage node at x_0 in Ref. 10's results, which is likely a result of the design process using this mode to trap all the energy in the tertiary's output capacitance (isolated-tertiary mode). While it's tempting to try to improve the crude approximation's agreement, it's not warranted for such a simple model that neglects the primary.

The corresponding uniform line for this magnifier is given by the effective parameters $x_0^*/H^* \approx 0.123$, $C_{\text{load}}/C_0^* \approx 0.219$, and $C_{\text{tap}}/C_0^* \approx 3.65$, and reproduces the three resonant frequencies on the bottom row of Table I to within 3% or better. Fig. 3 show profiles for this line, which agree reasonably well with those in Fig. 5. This uniform line falls in the large tap (but weak load) regime discussed earlier.

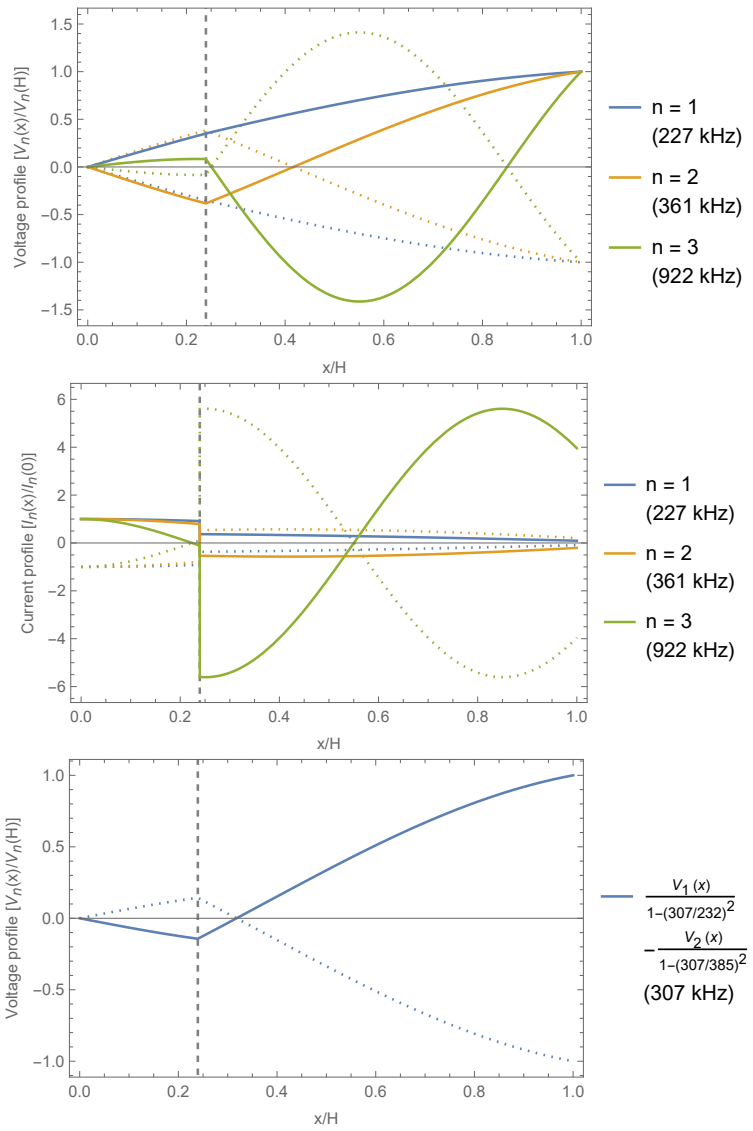

FIG. 5. Spatial profiles for the example magnifier of Ref. 11. Voltage (top) and current (middle) profiles for the first three modes, normalized at the top and bottom, respectively. Approximation (middle) of a voltage profile driven by the primary circuit. The dashed vertical line marks x_0, and the dotted curves are reflections of the solid curves to guide the eye. These profiles agree reasonably well with more accurate simulations in Ref. 10 that include the primary circuit.

III. DISCUSSION

This note presented a toy model for the normal modes of the coupled secondary and tertiary of a Tesla magnifier (or a shorted transmission line with internal and terminating capacitive loads). The model seemed to work well in comparison with a real magnifier and a more sophisticated simulation. It also provides another interesting example of nonharmonic Fourier series.

However, my original interest in this was to see if the curious appearance of a mode

doubling in the simulation of Ref. 10 might indicate a more general phenomenon across the mode structure of this and related systems. Unfortunately, this does not seem to be the case. The general structure seems rather complicated for magnifiers, even excluding the primary, though this note offers several limiting behaviors to guide intuition.

That said, mode doublings do indeed occur, as discussed above. Of particular interest is the regime of large tap capacitance, which tends to feature a pair of lowest modes that are hybridized, such as with the 3:4:5 magnifier or in Fig. 2(top right) for $C_{\text{tap}}/C_0 \gtrsim 40$. I suspect that this large-tap regime is common in actual magnifiers, and I suspect that the design procedure of Ref. 12 tends to use this regime to generate an isolated-tertiary mode. Otherwise, localized mode doublings do indeed occur in chance hybridizations from the tap capacitance (and likely with the primary circuit, if it was included). For example, see the (very narrowly) avoided crossings in Fig. 2(top right) for the 2nd and 3rd modes.

Interestingly, the large-tap regime seems related to an intriguing bit of lore I've encountered while reading about magnifiers, which is that the tertiary is often said to act as an isolated quarter-wave resonator. Of course, the careful design procedure of Ref. 12 can definitely achieve this momentarily as energy is briefly isolated in the tertiary alone. That said, I was generally skeptical of this idea in the past, because the secondary and tertiary are directly connected and thus strongly coupled. However, one of the limiting behaviors shown in this note is the ability of a large tap capacitance to asymptotically sever the secondary and tertiary. Thus, while in the large-tap regime, but before reaching that limit, it seems likely that one of the modes will tend to approximate an isolated tertiary (with topload).

For a derivation of a lumped-element equivalent circuit for magnifiers, please see Ref. 2.

REFERENCES

[1]Wikipedia has a brief description: `https://en.wikipedia.org/wiki/Tesla_coil#Number_of_coils`

[2]B. H. McGuyer, "Deriving the equivalent circuit of a Tesla magnifier," technical note, 2024. Available online: `https://bartmcguyer.com/notes/note-17-MagnifierEquations.pdf`

[3]F. M. Bieniosek, "Triple resonance pulse transformer circuit," Review of Scientific Instruments **61**, 1717–1719 (1990). DOI: 10.1063/1.1141138

[4]J. R. Reed, "Analytical expression for the output voltage of the triple resonance Tesla transformer," Review of Scientific Instruments **76**, 104702 (2005). DOI:10.1063/1.2093764

[5]J. R. Reed, "Designing triple resonance Tesla transformers of arbitrary modal frequency ratio," Review of Scientific Instruments **77**, 033301 (2006). DOI:10.1063/1.2173949

[6]M. Li, F. Zhang, C. Liang, and Z. Xu, "Development of 600 kV triple resonance pulse transformer," Review of Scientific Instruments **86**, 064707 (2015). DOI:10.1063/1.4922825

[7]B. H. McGuyer, "Deriving the equivalent circuit of a Tesla coil," technical note, 2020. Available online: `https://bartmcguyer.com/notes/note-11-TcEquations.pdf`

[8]B. H. McGuyer, "Transmission-line models for single-layer solenoid inductors," technical note, 2021. Available online: `https://bartmcguyer.com/notes/note-13-CoiledLines.pdf`

[9]B. H. McGuyer, "Nonharmonic Fourier series," technical note, 2023. Available online: `https://bartmcguyer.com/notes/note-10-NonharmonicFourier.pdf`

[10]Tesla Coil Mailing List post (and thread), "Re: [TCML] Magnifier topics", by Paul Nicholson, 2/14/2010.
Available online: https://www.pupman.com/listarchives/2010/Feb/msg00187.html

[11]Webpage, "A 6th-order Tesla Magnifier," by Antonio Carlos M. de Queiroz, 5/12/2003.
Available online: https://www.coe.ufrj.br/~acmq/tesla/mag345.html

[12]Webpage, "Designing a Tesla Magnifier," by Antonio Carlos M. de Queiroz, 10/8/2003, and references.
Available online: https://www.coe.ufrj.br/~acmq/tesla/magnifier.html

[13]Webpage, "A transformerless Tesla coil," by Antonio Carlos M. de Queiroz, 8/26/2006.
Available online: https://www.coe.ufrj.br/~acmq/tesla/mres4.html

[14]B. H. McGuyer, "Test of the Miller self-capacitance of a solenoid inductor," technical note, 2021.
Available online: https://bartmcguyer.com/notes/note-12-MillerCapTest.pdf